A Substrate Selectivity and Inhibitor Design Lesson from the PDE10−cAMP Crystal Structure: A Computational Study

Justin Kai-Chi Lau,* Xiao-Bo Li, and Yuen-Kit Cheng

Department of Chemistry, The Hong Kong Baptist University, Waterloo Road, Kowloon Tong, Kowloon, Hong Kong, China

Received: November 24, 2009; Revised Manuscript Received: February 10, 2010

Phosphodiesterases (PDEs) catalyze the hydrolysis of second messengers cAMP and cGMP in regulating many important cellular signals and have been recognized as important drug targets. Experimentally, a range of specificity/selectivity toward cAMP and cGMP is well-known for the individual PDE families. The study reported here reveals that PDEs might also exhibit selectivity toward conformations of the endogenous substrates cAMP and cGMP. Molecular dynamics simulations and free energy study have been applied to study the binding of the cAMP torsional conformers about the glycosyl bond in PDE10A2. The computational results elucidated that PDE10A2 is energetically more favorable in complex with the *syn* cAMP conformer (as reported in the crystal structure) and the binding of *anti* cAMP to PDE10A2 would lead to either a nonreactive configuration or significant perturbation on the catalytic pocket of the enzyme. This experimentally inaccessible information provides important molecular insights for the development of effective PDE10 ligands.

Introduction

Phosphodiesterases (PDEs), thus far encoded by 21 genes categorized into 11 families in humans, are important intracellular enzymes for the regulation of the second messenger 3′,5′-cyclic adenosine/guanosine monophosphate (cAMP/cGMP) in response to a variety of stimuli.[1–5] Through hydrolysis of the 3′-cyclic phosphate bond catalyzed by PDE, cAMP or cGMP is being inactivated into its acyclic phosphate product. Inhibiting an individual PDE specifically maintains the response to a particular stimulus in certain biological (pathological) conditions, and thus, PDEs have been scrutinized as important therapeutic targets.[6–12] One of the most successful synthetic PDE inhibitors is exemplified by sildenafil, which is an inhibitor of PDE5 effective for the treatments of male erectile dysfunction and pulmonary hypertension.[13,14]

The domain structure of each PDE can be functionally partitioned into three regions in general: an N-terminal splicing region, a regulatory domain, and a C-terminal catalytic domain. Endogenous substrate cAMP/cGMP binds to the catalytic pocket consisting of a purine-binding site and a bimetallic reactive center located at the other end, where hydrolysis takes place. Notably, there is an invariant glutamine (invariant gln) forming hydrogen bonds with the purine ring of the substrate at the apex of the purine-binding site.[15–18] The divalent metal ions in the bimetallic center found in all PDEs are putatively bridged by a hydroxide ion acting as a nucleophile.[19,20] Although the general structural aspects of the catalytic pockets across the PDE families are very similar, the superfamily still shows trimodal specificity toward the two cyclic nucleotides. PDE4, -7, and -8 are specific for cAMP, while PDE5, -6, and -9 are for cGMP, and the rest are dual-specific.[4,7] A "glutamine switch" hypothesis[21] had been proposed to explain the specificities of PDEs. This hypothesis is based on the crystal structures cocrystallized with inhibitors/products of PDE4 and PDE5 that the "locked" invariant gln is able to form two hydrogen bonds with cAMP but only one with cGMP in cAMP-specific PDEs and vice versa in cGMP-specific PDEs due to the difference in the hydrogen-bonding patterns of adenine and guanine. For the dual-specific PDEs, the side-chain amido group of the invariant gln is able to rotate "freely", forming two hydrogen bonds with either substrate. This seems consistent with the dual-specific PDE1B and PDE3B crystal structures in which the invariant gln side chains have no inter-residue locking hydrogen bonds and thus are rather free to rotate.[21,22] In this hypothesis, the orientations of the purine base, sugar, and the cyclic phosphate group of both cAMP and cGMP in the catalytic pockets are assumed to be similar. This mechanistic generalization, however, cannot fully explain the mutagenesis experiments in which the mutation of the locking Gln775 of the invariant gln (Gln817) in PDE5A1 to alanine weakened only the affinity toward cGMP but without an expected concomitant increase in that of cAMP.[23] Further, Ke et al. based on endogenous substrates cAMP/cGMP in the recently solved PDE10A2 crystal structures have also observed oddities inconsistent with the glutamine switch mechanism and hence suggested that the substrate specificity of PDE should rather be determined by multiple elements including the subtle variation of amino acids in the catalytic pocket.[17] Undoubtedly, the invariant gln plays a key role in the binding of nucleotides, but in light of these latter puzzling experimental findings, its absolute importance as a "switch" selecting between cAMP and cGMP needed to be reviewed in a more quantitative manner, specifically with respect to PDE10 reported here in this work.

PDE10 is highly expressed in the brain striatum,[24–27] and its selective inhibitor papaverine, an isoquinoline alkaloid, for the treatment of psychosis has been suggested.[28–30] The catalytic domains of the PDE10A2 bound with either cAMP or cGMP are found to be reactive.[17] This is consistent with the known physiological dual specificity of PDE10.[31–33] However, the side chain of the invariant gln is locked (in the cAMP-specific binding mode with respect to the gultamine switch hypothesis) by a neighboring residue and also on the other side by a water molecule hydrogen-bonded to two other residues. Hence, it is not free to rotate and indeed no reorientation of the invariant

* Corresponding author. E-mail: justin@hkbu.edu.hk. Phone: +852 3411 5815.

10.1021/jp911156g © 2010 American Chemical Society
Published on Web 03/29/2010

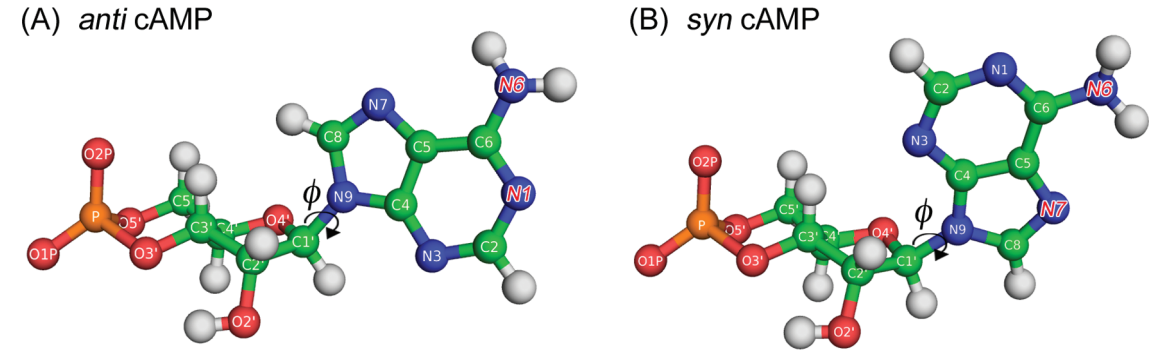

Figure 1. Conformers of cAMP and the torsional angle ϕ defined by O4′−C1′−N9−C8: (A) *anti* cAMP, $\phi \sim 20°$, the N6 and N1 atoms are putatively involved in the hydrogen bonding with the invariant glutamine residue in PDE4; (B) *syn* cAMP, $\phi \sim -120°$, the N6 and N7 atoms are putatively involved in the hydrogen bonding with the invariant glutamine residue in PDE10.

gln is observed in the PDE10A2 crystal structures containing cGMP relative to that containing cAMP.[17] The cGMP molecule can only form one hydrogen bond with the invariant gln, and thus, dual-specific PDE10A2 does not ideally abide to the glutamine switch hypothesis in the sense that the switch can rotate to accommodate both cAMP and cGMP favorably. More interestingly, bound cAMP in the PDE10A2 crystal structure is definitively "forced" into the *syn* conformation despite the fact that cAMP exists in solution equilibrium *syn* versus *anti* of percentage ratio 30:70.[34] This is in stark contrast to the cAMP-specific PDE4 (and presumably other cAMP-binding PDEs) structure in which the ligand is in the *anti* conformation and has a different hydrogen-bond base pairing with the invariant gln (Figure 1).[16] This required binding mode of cAMP in PDE10A2 may lead to the fact that PDE10 possesses a low affinity toward the PDE4 inhibitor rolipram.[10]

There exists quite a few recent computational studies covering several important aspects of PDEs.[19,20,35–41] For example, molecular dynamics (MD) simulations and hybrid quantum mechanics/molecular mechanics (QM/MM) calculations have been employed in characterizing the bridging ligand between the two metal ions in PDE.[19,20] Wierzbicki et al. have also applied the QM/MM method to study the hydrolysis of cAMP in PDE4[37] and the cyclic nucleotide recognition in different PDEs by using truncated models derived from crystal structures.[38,39] Zagrovic et al. have employed thermodynamic integration to study the binding affinities of several inhibitors toward PDE5.[40] More recently, Zhan et al. have compared the binding affinities of several inhibitors toward PDE2 by using MD simulations and molecular mechanics/Poisson−Boltzmann surface area (MM/PBSA) methods.[41] While most of these theoretical studies are based on the apo, truncated, or inhibitor-bound crystal structures, more interesting computational studies as reported here will come from the PDE crystal structures in complex with the intact endogenous substrates just released.

In this work, the binding modes of *syn* and *anti* cAMP inside the catalytic domain of PDE10A2 (PDE10 hereafter unless stated otherwise) have been studied by using MD simulations at the atomistic level. The key question and lesson to be learned here is why PDE10 selects the *syn* rather than the seemingly more preferred (thermodynamically) *anti* cAMP conformer as observed in PDE4. Further, considered that the invariant gln is already locked in the cAMP-specific binding mode, why PDE10 also and be able to bind cGMP unlike of the other cAMP-specific PDEs in acting as a dual-specific PDE biologically instead. The hypothetical *anti* cAMP conformers in PDE10 have been modeled from the crystal structure through conformational conversion of the substrate operationally. This operational *syn* to *anti* conversion of cAMP inside protein is a statistically rare event within the time scale accessible to the conventional MD simulation. Hence, the "umbrella sampling" methodology has been applied to enhance the sampling.[42,43] The importance of the conformation of cyclic nucleotides in relation to PDE specificity toward them and thus implications in inhibitor design for PDE10 is discussed after the results are presented.

Methodology

Simulation Details. All simulations were performed using the AMBER(v9.0) package with the AMBER force field for the amino-acid residues.[44] The initial structure of the PDE10 catalytic domain was obtained from the Protein Data Bank (PDB code: 2OUY) which is a D564N mutant shown to be representative of the native protein structurally.[17] On the basis of this structure, the root-mean-square deviation (rmsd) of the protein backbone between the wild type and D564N models after minimization was calculated to be only 0.372 Å. Therefore, the model based on the wild-type sequence was used for all subsequent simulations and analyses. The parameters of cAMP and the bridging hydroxide anion were prepared by using the generalized force-field "antechamber" module in AMBER.[45,46] Three Na^+ counterions were added to the system to ensure charge neutrality, and the system was solvated by 13 304 TIP3P[47] water molecules. Energy minimization was carried out prior to simulation in each case to remove artificial forces of the initial crystal structure relative to the force field adopted. MD simulation of 200 ps was then carried out at constant temperature (300 K) and volume for equilibration (NVT ensemble). The SHAKE algorithm[48] was used to constrain the bonds connecting hydrogen and heavy atoms, and a time step of 2 fs was used for the integration of equations of motion. Further equilibration of 2 ns was carried out at a constant temperature and pressure condition (NPT ensemble) before starting production simulation. The operational definition of hydrogen bond used in this work and the corresponding relevant statistics of the simulation structures are complied for reference (Table S1 in the Supporting Information).

Umbrella Sampling. The torsional angle (ϕ) which is defined by O4′−C1′−N9−C8 in cAMP (Figure 1) was used as the collective variable (the only parametrically varied internal coordinate in the whole system) to characterize the *syn* to *anti* conversion of cAMP. The conversion pathway was divided into 19 (12 for counterclockwise and 7 for clockwise simulations) overlapping windows. An artificial bias potential $U(\phi)$ was applied to restrain the sampling of the collective variable in each window, while the rest of the system was not biased. The probabilistic distribution of ϕ in each window along the

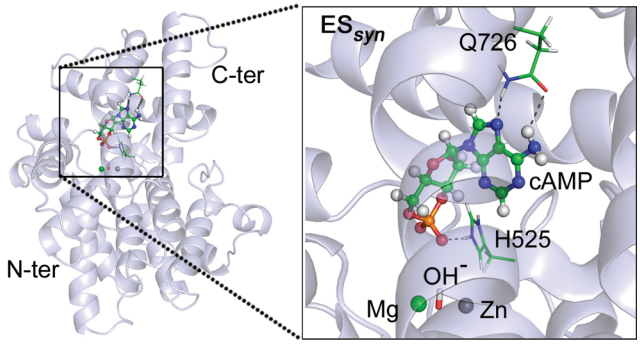

Figure 2. Structures of ES$_{syn}$: the entire *syn* cAMP is bound inside the catalytic pocket and forms hydrogen bonds with the residues Gln726 and His525.

trajectory, $p(\phi)$, was determined, and the potential of mean force $W(\phi)$ was calculated by

$$W(\phi) = k_B T \ln p(\phi) \quad (1)$$

where k_B and T are the Boltzmann's constant and the temperature, respectively.

The bias potential is represented by a simple-harmonic-like equation:

$$U(\phi) = k[\phi - \phi_0]^2 \quad (2)$$

where $k = 30$ kcal mol^{-1} rad^{-2} is the force constant which describes the hardness of the bias potential and ϕ_0 is the center (minimum) of the potential in each window. By sampling around ϕ_0 in each window, a complete conversion has been sampled and the final free energy surface was recovered by combining the piecewise results from each window using the weighted histogram analysis method (WHAM).[49] A simulation of 3.5 ns was carried out in each window for the collection of relevant statistics.

Results

***syn* cAMP in PDE10.** The equilibrium structure of the enzyme PDE10 in complex with the substrate *syn* cAMP after simulation is shown in Figure 2 (ES$_{syn}$). The rmsd of the protein backbone during the simulation in reference to the crystal structure was monitored (Figure S1 in the Supporting Information). The system was well equilibrated, and the overall structure highly resembles the crystal structure. The interactions between the substrate and the enzyme found in the simulation are consistent with the experimental structure.[17] The purine ring of cAMP is sandwiched between Phe729 and Ile692 in the purine-binding site. N6 and N7 of adenine form hydrogen bonds with the amido side chain OE1 and NE2 of the invariant gln (Gln726), respectively (Figure 3A). At the same time, the invariant gln side chain is locked by the neighboring Tyr693 and a water molecule (bound to Tyr730 and Trp762) through hydrogen bonds which were also observed in the crystal structure (Table S1 in the Supporting Information). At the other end of the bimetallic center, the oxygen (O2P) in the cyclic phosphate group forms a strong hydrogen bond with the neighboring His525 residue. This histidine has been suggested to function as a proton donor in the hydrolysis reaction.[15,37,50] It is worth mentioning that both metal ions are hexa-coordinated in the simulation the same as that deduced from the crystal structure with a hydroxide ion bridging in between them (Figure 3A). The small fluctuation of the torsion ϕ in cAMP during the simulation (Figure S2, Supporting Information) suggests a stable *syn* conformation of cAMP inside the catalytic pocket of PDE10. The overall agreement between the simulation and the crystal structure renders the subsequent calculations more reliable.

Modeling of *anti* cAMP in PDE10. Umbrella sampling was used to enable adequate statistics being sampled in the simulation (Figure S3, Supporting Information) and the calculation started at the ES$_{syn}$ configuration pre-equilibrated as reported above. ϕ (Figure 1) was gradually varied by applying a bias potential in each simulation window until the final *anti* geometry of cAMP was obtained in both rotational directions (case 1, counterclockwise; case 2, clockwise). In the thermodynamic limit, one would obtain the same global minimum structure when a given molecule is subjected to rotation in either direction about a rotatable bond. In fact, in the umbrella sampling simulation of a simple system as the infinitely dilute *syn* cAMP in water medium, the same final (*anti*) structures were obtained in both rotational directions. However, quite contrary to the simple cases, the molecular entity would instead encounter a spatially restricted anisotropic environment inside an enzyme, and consequently bond rotation in opposite rotational directions would lead to intermediate states encountering different *kinetic* barriers likely representing the different binding poses (configurations) of ligand even in the same conformation. Hence, calculations have been carried out in both rotational directions and indeed leading to two *anti* configurations in the catalytic pocket as detailed below separately. We have to emphasize that the exact molecular process of how *anti* cAMP in solution achieves the *syn* conformation in the crystal structure is not of our concern here. PDE10 may evolutionarily select the minor conformer *syn* cAMP directly from solution prebinding or via induced conversion along the entering path. The particular *syn*/*anti* conversion pathways adopted here are merely operational in facilitating robust free energy estimations of the two conformers at the conversion end-points. It is sensible starting the conversion based on the crystal structure (i.e., ES$_{syn}$). Docking the *syn* or *anti* ligand directly into the pocket allowing protein flexibility will likely lead to the same results if done properly albeit much less convenient computationally, even if possible, in estimating the free energy values robustly.

Case 1 (Counterclockwise). The torsion ϕ of cAMP started at about $-120°$ corresponding to ES$_{syn}$. The final free energy surface for the conformational conversion of cAMP inside PDE10 is summarized in Figure 4 (the top curve). A local energy minimum at about 15° is predicted corresponding to an *anti* configuration of cAMP in PDE10 (ES$_{anti}$). On the basis of this minimum state, an MD simulation has been carried out and the equilibrium structure obtained (Figure 3B), indicating that the interaction between the adenine and the invariant gln remains essentially unchanged. However, the cyclic phosphate group rotated out from the bimetallic reactive center in order to attain this *anti* configuration. The hydrogen bond between the phosphate and His525 was lost. Instead, a strongly solvated cyclic phosphate group is observed. The radial distribution functions of the phosphate oxygens with respect to water molecules (Figure S4, Supporting Information) imply that the phosphate group was stabilized by the proximal solvent water medium rather than interacting with other protein residues, and the phosphate group in ES$_{anti}$ was more exposed to the solvent than that in ES$_{syn}$, showing similarity as seen in some inhibitors with the polar moieties dangling out to the solvent. The protein backbone rmsd of this *anti* cAMP configuration is comparable

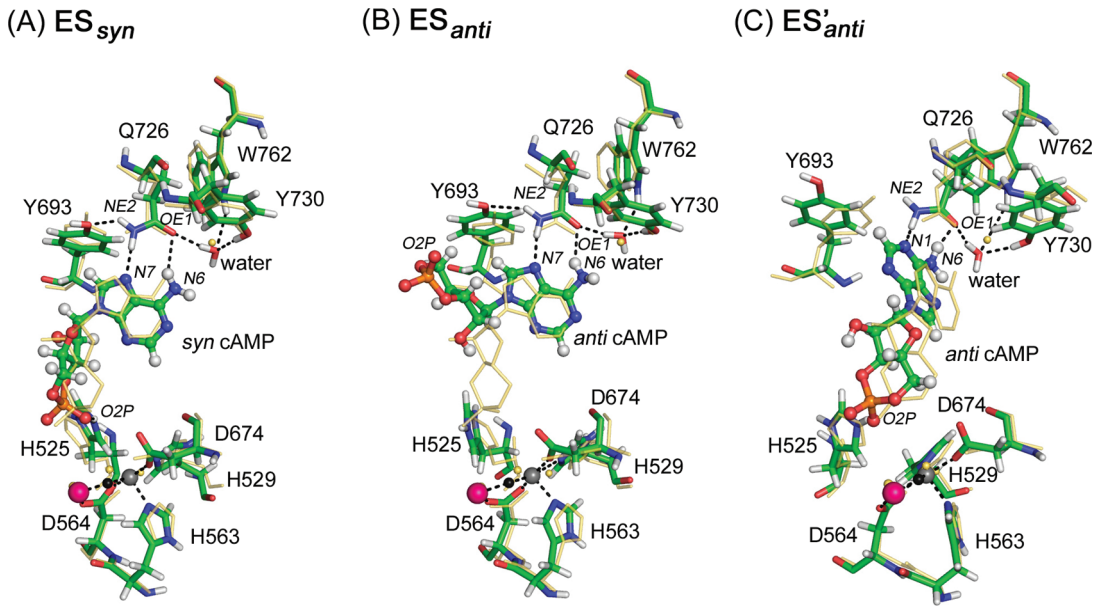

Figure 3. Binding modes of cAMP in the catalytic pocket of PDE10: (A) ES$_{syn}$, (B) ES$_{anti}$, and (C) ES′$_{anti}$. Mg^{2+} and Zn^{2+} are represented by the larger purple and gray spheres at the bottom, respectively. Water molecules coordinated to the two metal ions are not shown for clarity. The hydroxide ion bridging the two metal ions is represented by a small black sphere. The crystal structure (2OUY) is aligned and shown as a light yellow stick (small isolated yellow ball for crystal water) for comparison. The observed crystal water bridging Y730 and W762 to the invariant gln Q726 is shown explicitly.

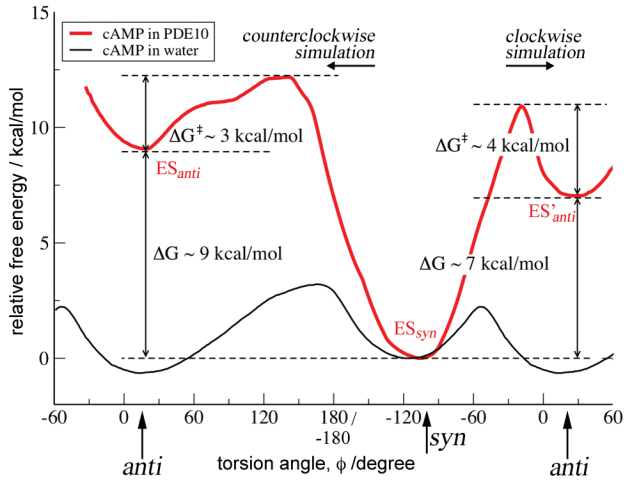

Figure 4. Free energy surface for the conformational conversion of cAMP in PDE10 subjected to counterclockwise and clockwise umbrella samplings (top curve) and in solution by itself (bottom curve).

to that with the *syn* cAMP in reference to the crystal structure (Figure S1, Supporting Information). From Figure 4, it can be concluded that ES$_{anti}$ is thermodynamically less stable than ES$_{syn}$ by ∼9 kcal mol^{-1}. In fact, the rotating out of the cyclic phosphate group of cAMP from the bimetallic center indicates that the substrate is not ready for hydrolysis to take place anymore.

For comparison, the conformational conversion of cAMP in "bulk" water medium was also calculated at 300 K (Figure 4, the bottom curve). The *anti* conformation of cAMP is instead slightly more stable (∼0.6 kcal mol^{-1}) than the *syn* conformation in solution and the barrier for the *anti* to *syn* conformation is less than 4 kcal mol^{-1} (for both rotational directions). The calculations based on X-ray and NMR results predict that the *anti* versus *syn* conformation of cAMP is of percentage ratio 70:30 in bulk water medium.[34] It corresponds to *anti* cAMP ∼0.5 kcal mol^{-1} more stable than the *syn* conformer (Table S2, Supporting Information). Our simulation results corroborate well with this experimental prediction.

Case 2 (Clockwise). The simulation again started at ES$_{syn}$ with ϕ varied in the opposite rotational direction this time. Inspecting the structure during sampling reveals that the cyclic phosphate group of cAMP tends to be "locked" inside the active site of the protein, but the purine adenine undergoes rotation leading to another *anti* cAMP configuration (ES′$_{anti}$) and the hydrogen bond between N7 of adenine and NE2 of Gln726 was replaced by N1 of adenine and NE2 of Gln726 by a flipping of the adenine ring (Figure 3C), resulting in a canonical cAMP-binding configuration found in the glutamine switch hypothesis though highly strained. However, the protein backbone rmsd of ES′$_{anti}$ with respect to the crystal structure shows a significantly larger deviation relative to that of ES$_{anti}$ (Figure S1, Supporting Information). Further inspecting the ES′$_{anti}$ structure reveals that the distance between the center of mass of the two metal ions and the side chain of the invariant gln is significantly longer than that of ES$_{syn}$ (>1 Å), implying that the native catalytic pocket is stretched vertically throughout the trajectory (Figure S5, Supporting Information). Consequently, the hydrogen bond between Gln726 and Tyr693 was lost (Table S1, Supporting Information) and the amido nitrogen group of the invariant gln residue deviated from the position relative to that of ES$_{syn}$ (Figure 3C). The structure indicates that *anti* cAMP in this configuration cannot be embedded entirely (base plus sugar−phosphate) inside the catalytic pocket of PDE10 without inducing major perturbation to the pocket. In fact, it is consistent with the preliminary modeling results that the phosphate oxygen of "fully embedded" *anti* cAMP clashes with the two water molecules coordinated with the metals ions found in the crystal structure.[17] The free energy surface in Figure 4 summarized that ES′$_{anti}$ is also thermodynamically less stable than ES$_{syn}$ (by ∼7 kcal mol^{-1}).

Discussions

Substrate Binding Specificity. The purine base of cAMP possesses two potential hydrogen-bond acceptors (N1 and N7) and one donor (N6) available to interact with the invariant gln side chain (Figure 1). cAMP exhibits two distinct binding modes

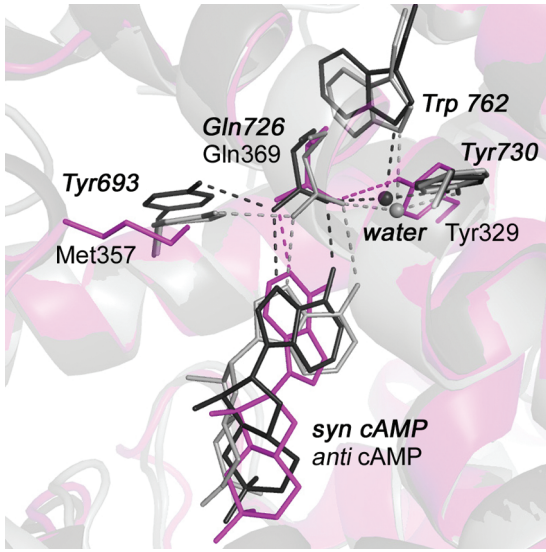

Figure 5. Superimposed crystal structures of PDE10 in complex with *syn* cAMP (2OUY, black) and PDE4 in complex with *anti* cAMP (2PW3, purple). The side chain of the invariant gln Gln726 in PDE10 is locked by neighboring Tyr693 and a water molecule bound to Tyr730 and Trp762. The side chain of the invariant gln Gln369 in PDE4 is locked by Tyr329 only. The simulated ES_{syn} is shown in gray for comparison. Bold and italicized labels are for PDE10. The rest of the protein structures are rendered as faded out ribbons, showing they are very similar structurally.

inside the catalytic pocket of PDE via *syn* (using N7 and N6 as in PDE10) or *anti* (using N1 and N6 as in PDE4) conformations as observed in crystal structures.[16,17] The latter is also found in most other crystal structures of the product AMP.[21] Despite both binding modes being hydrolytically active in the respective PDEs, the spatial requirement for accommodating these two torsional conformers in the pocket is different. The *anti* conformer requires a more extended vertical dimension of the pocket than the *syn* conformer in order to maintain all of the important interactions in PDE10 (Figure S6a, Supporting Information). The hydrogen bond between N6 of cAMP and OE1 of the invariant gln is somewhat weakened in the PDE4 crystal structure.[16] The hydrogen bond distance is 3.78 Å compared with 3.11 Å found in a product AMP crystal structure,[21] but the binding configurations are almost identical (Figure S6b, Supporting Information). Comparing PDE4 and PDE10, only in PDE10 are both the amino and carbonyl groups of the invariant gln side chain locked by the neighboring residue (Tyr693) and a water molecule through hydrogen bonds, respectively (Figure 5). Hence, this spatially restricted catalytic pocket of PDE10 only allows the binding of the more compact *syn* cAMP (ES_{syn}) even though the *syn* conformation is thermodynamically less dominant in solution. The binding of the entire *anti* conformer inside the pocket is less favorable (by ~7 kcal mol^{-1}, Figure 4) with the hydrogen-bonding network of the invariant gln being perturbed as predicted (in ES'_{anti}). In PDE4D, only the amido oxygen of the invariant gln (Gln369) is locked by the neighboring residue (Tyr329) through direct hydrogen bonding. Met357 in PDE4D (corresponds to Tyr693 in PDE10) is not able to form a hydrogen bond with the amido nitrogen of the invariant gln Gln369 (Figure 5).[16] Thus, the catalytic pocket of PDE4 is in principle more flexible vertically than that of PDE10 and thus binds the dominant solution form (*anti*) of cAMP in the cAMP-specific binding mode according to the glutamine switch hypothesis. The crystal structures of other PDE families in complex with cAMP are not solved yet. However, early studies suggested PDE1 and -2 prefer to bind with *syn* cAMP also.[51] Inspecting their apo and inhibitor-binding structures found that either *anti* cAMP may clash with the side chain of His369 (PDE1)[21] or the amido nitrogen of the invariant gln is locked by a water molecule (PDE2),[52] making them less favorable to bind with the *anti* conformers (not shown).

The favorable binding of cGMP in cGMP-specific PDEs is to form double (barely triple) hydrogen bonds with the invariant gln amido group "switched" and being locked in an opposite orientation as observed in the crystal structure of PDE9 where cGMP is in the *anti* conformation in accord with the glutamine switch hypothesis.[18] However, cGMP in the crystal structure of PDE10 can only be fitted into the pocket in a *syn* geometry, forming a single hydrogen bond (using N7 instead) with the invariant gln, since the "switch" is still locked in the cAMP-specific binding mode.[17] The weaker binding of cGMP in PDE10 is nicely reflected by the much higher K_m value compared to that of cAMP as reported experimentally in PDE10A2 (4.4 μM vs 56 nM).[17] Interestingly, cGMP-specific PDE9 selects the thermodynamically less dominant *anti* cGMP (5% population in solution)[34] in order to maintain the double (or triple) hydrogen bonds with the invariant gln. Hence, there is a delicate balance between the hydrogen bonds and the glycosyl torsion preference of substrate binding.

Inhibitor Binding. The importance of the hydrogen-bond network around the invariant gln Gln726 in PDE10 in determining the exact binding properties of endogenous substrate cAMP and cGMP immediately points to important implications in inhibitor design. Therefore, we have compared the available crystal structures of PDE10−inhibitor complexes in light of our calculations for possible molecular insights. Recently, Chappie et al.[53] have obtained the crystal structure of PDE10 in complex with a tetrahydroisoquinolinyl dimethoxyquinazoline derivative (PDB: 2O8H) which is derived from the PDE10 inhibitor papaverine (Figure S7a, Supporting Information). From the crystal structure, the dimethoxyquinazoline moiety is located below the invariant gln, leaving the remaining part of the molecule (weakly polar) pointing out from the catalytic pocket, and almost void of any interaction with the bimetallic center. Both of the methoxyl groups form hydrogen bonds with the amido nitrogen of the invariant gln which is a rather common characteristic of PDE inhibitors. It is noted that the hydrogen-bond interactions between the side chain of the invariant gln and the surrounding residues remain intact upon the binding of the inhibitor as in ES_{syn} (Figure S7a, Supporting Information). In fact, the same hydrogen-bond network around the invariant gln is also observed in the crystal structures of a recent work by Verhoest et al. reporting a novel class of PDE10 inhibitors.[54] This novel inhibitor class (PDB: 3HQW) does not form a hydrogen bond with the conserved invariant gln Gln716 (Gln726 in human PDE10) directly (Figure S7b, Supporting Information). Instead, the side chain of the amido nitrogen of the invariant gln is positioned directly above the center of the methoxyphenyl groups of the inhibitor, forming an amino−π interaction.[54] In addition, the nitrogen atom in the imidazole of the inhibitor binds to Tyr683 (Tyr693 in human PDE10) through hydrogen bonding. Hence, the position of Tyr683, i.e., the preservation of the hydrogen-bond network around the invariant gln is important in the binding (Figure S7b, Supporting Information). These experimental observations are in line with our modeling results that the maintenance of the hydrogen bonds between Tyr693 and Gln726 is crucial for effective substrate/inhibitor binding with the exception found in the recent crystal structure of PDE10 cocrystallized with papaverine (PDB: 2WEY).[55] However, this structure may suffer from an artifact of crystal

contacts in the cross-link crystal as described by the authors. Papaverine and its derivatives are more potent than the PDE4−inhibitor rolipram toward PDE10.[10] Modeling of rolipram inside PDE10 found that the rigid cyclopentyl group in rolipram is in close contact to Tyr693, while it is only a methoxyl group in the corresponding position of papaverine (Figure S8, Supporting Information). The placement of rolipram in PDE10 with the orientation as observed in PDE4[21] (PDB: 1TBB) will inevitably perturb the hydrogen bond between Tyr693 and the invariant Gln726 significantly, and thus, rolipram is indeed a poor inhibitor toward PDE10.[10] Therefore, the future PDE10 inhibitor development should take consideration to preserve the hydrogen-bond network between the invariant gln Gln726 and the surrounding scaffolding residues. The inhibitor-binding modes observed in the crystals of papaverine and its derivative in PDE10 are reminiscent of ES_{anti} in our calculation (Figure S7a, Supporting Information). However, in ES_{anti}, the adenine is able to form double hydrogen bonds with the side chain of the invariant gln Gln726, while the two methoxyl groups of the inhibitor share the same hydrogen-bond donor (amido nitrogen) from the invariant gln. This double hydrogen-bond pattern in ES_{anti} may be a desirable aspect for the development of high-affinity PDE10 inhibitors in view of the unswitchable invariant gln, eliminating the need to consider the fluctuation of the hydrogen-bonding pattern. In comparison, inhibitor design further optimized the interaction with the bimetallic center (as in ES'_{anti}) will gain more affinity in terms of free energy (very crudely 2 kcal mol^{-1} comparing ES'_{anti} vs ES_{anti}, see Figure 4). However, additional polar charged groups must be incorporated inevitably that will likely lead to undesirable pharmacokinetic properties.

Conclusion

Apart from the specificity (or selectivity to be precise) toward substrates cAMP/cGMP, PDE families also demonstrate selectivity toward the conformations (*syn* versus *anti*) of the same substrate. Crystal studies reveal that cAMP is in the minor solution *syn* conformation in the catalytic pocket of PDE10 but *anti* in PDE4. From modeling, the perturbation of the catalytic pocket upon binding of the hypothetical *anti* cAMP in PDE10 (ES'_{anti}) in comparison with the observed *syn* form provides useful molecular insights for the effective design of PDE10 inhibitors. Specifically, the integrity of the inter-residue interactions (mainly hydrogen bonds) proximal to the invariant gln is revealed to be deterministic for the preferences of the *syn* cAMP and *syn* cGMP in PDE10 as well as the varying inhibitor selectivity reported thus far. Because of this stable interlocking constraint on the invariant gln, though PDE10 is in the cAMP-specific binding mode, binding substrate cAMP is forced into the more compact *syn* conformation. However, cGMP naturally adopts this compact *syn* conformation and is able to form a unique stabilizing hydrogen bond with the invariant glutamine. This leads to the observable biological dual specificity of PDE10 in reality which is seemingly incompatible with the dual-specific PDE within the framework of the glutamine switch hypothesis. Hence, PDE10A2 can rather be named cAMP-specific in the context of the glutamine switch model though possessing strong scaffolding interactions constricting the invariant gln lending a weak but unexpected binding mode to cGMP. It would then be interesting to reason for the inexistence of this cGMP-binding mode in other PDEs formally classified as cAMP-specific.

Acknowledgment. This work is supported by the HKBU internal grant FRG/07-08/II-69. Computing support from Mr. Morris Law at the High Performance Cluster Computing Center at HKBU is cordially appreciated. Part of the computation was done at the NERSC in USA, and J.K.-C.L. would like to acknowledge this.

Supporting Information Available: Details of the simulation results. This material is available free of charge via the Internet at http://pubs.acs.org.

References and Notes

(1) Sutherland, E. W. *Science* **1972**, *177*, 401.
(2) Conti, M.; Beavo, J. *Annu. Rev. Biochem.* **2007**, *76*, 481.
(3) Omori, K.; Kotera, J. *Circ. Res.* **2007**, *100*, 309.
(4) Mehats, C.; Andersen, C. B.; Filopanti, M.; Jin, S. L. C.; Conti, M. *Trends Endocrinol. Metab.* **2002**, *13*, 29.
(5) Soderling, S. H.; Beavo, J. A. *Curr. Opin. Cell Biol.* **2000**, *12*, 174.
(6) Menniti, F. S.; Faraci, W. S.; Schmidt, C. J. *Nat. Rev. Drug Discovery* **2006**, *5*, 660.
(7) Bender, A. T.; Beavo, J. A. *Pharmacol. Rev.* **2006**, *58*, 488.
(8) Ke, H. M.; Wang, H. C. *Curr. Top. Med. Chem.* **2007**, *7*, 391.
(9) Lugnier, C. *Pharmacol. Ther.* **2006**, *109*, 366.
(10) Rotella, D. P. In *Comprehensive Medicinal Chemistry II*; Moos, W. H., Ed.; Elsevier: Amsterdam, The Netherlands, 2007; Vol. 2, p 919.
(11) Flocco, M.; Brown, D. G. In *Comprehensive Medicinal Chemistry II*; Mason, J. S., Ed.; Elsevier: Amsterdam, The Netherlands, 2007; Vol. 4.
(12) Huang, Z.; Mancini, J. A. *Curr. Med. Chem.* **2006**, *13*, 3253.
(13) Corbin, J. D.; Francis, S. H. *Int. J. Clin. Pract.* **2002**, *56*, 453.
(14) Galie, N.; Ghofrani, H. A.; Torbicki, A.; Barst, R. J.; Rubin, L. J.; Badesch, D.; Fleming, T.; Parpia, T.; Burgess, G.; Branzi, A.; Grimminger, F.; Kurzyna, M.; Simonneau, G.; Grp, S. S. *N. Engl. J. Med.* **2005**, *353*, 2148.
(15) Xu, R. X.; Hassell, A. M.; Vanderwall, D.; Lambert, M. H.; Holmes, W. D.; Luther, M. A.; Rocque, W. J.; Milburn, M. V.; Zhao, Y. D.; Ke, H. M.; Nolte, R. T. *Science* **2000**, *288*, 1822.
(16) Wang, H. C.; Robinson, H.; Ke, H. M. *J. Mol. Biol.* **2007**, *371*, 302.
(17) Wang, H. C.; Liu, Y. D.; Hou, J.; Zheng, M. Y.; Robinson, H.; Ke, H. M. *Proc. Natl. Acad. Sci. U.S.A.* **2007**, *104*, 5782.
(18) Liu, S. P.; Mansour, M. N.; Dillman, K. S.; Perez, J. R.; Danley, D. E.; Aeed, P. A.; Simons, S. P.; LeMotte, P. K.; Menniti, F. S. *Proc. Natl. Acad. Sci. U.S.A.* **2008**, *105*, 13309.
(19) Zhan, C. G.; Zheng, F. *J. Am. Chem. Soc.* **2001**, *123*, 2835.
(20) Xiong, Y.; Lu, H. T.; Li, Y. J.; Yang, G. F.; Zhan, C. G. *Biophys. J.* **2006**, *91*, 1858.
(21) Zhang, K. Y. J.; Card, G. L.; Suzuki, Y.; Artis, D. R.; Fong, D.; Gillette, S.; Hsieh, D.; Neiman, J.; West, B. L.; Zhang, C.; Milburn, M. V.; Kim, S. H.; Schlessinger, J.; Bollag, G. *Mol. Cell* **2004**, *15*, 279.
(22) Scapin, G.; Patel, S. B.; Chung, C.; Varnerin, J. P.; Edmondson, S. D.; Mastracchio, A.; Parmee, E. R.; Singh, S. B.; Becker, J. W.; Van der Ploeg, L. H. T.; Tota, M. R. *Biochemistry* **2004**, *43*, 6091.
(23) Zoraghi, R.; Corbin, J. D.; Francis, S. H. *J. Biol. Chem.* **2006**, *281*, 5553.
(24) Seeger, T. F.; Bartlett, B.; Coskran, T. M.; Culp, J. S.; James, L. C.; Krull, D. L.; Lanfear, J.; Ryan, A. M.; Schmidt, C. J.; Strick, C. A.; Varghese, A. H.; Williams, R. D.; Wylie, P. G.; Menniti, F. S. *Brain Res.* **2003**, *985*, 113.
(25) Kotera, J.; Sasaki, T.; Kobayashi, T.; Fujishige, K.; Yamashita, Y.; Omori, K. *J. Biol. Chem.* **2004**, *279*, 4366.
(26) Xie, Z.; Adamowicz, W. O.; Eldred, W. D.; Jakowski, A. B.; Kleiman, R. J.; Morton, D. G.; Stephenson, D. T.; Strick, C. A.; Williams, R. D.; Menniti, F. S. *Neuroscience* **2006**, *139*, 597.
(27) Coskran, T. M.; Morton, D.; Menniti, F. S.; Adamowicz, W. O.; Kleiman, R. J.; Ryan, A. M.; Strick, C. A.; Schmidt, C. J.; Stephenson, D. T. *J. Histochem. Cytochem.* **2006**, *54*, 1205.
(28) Siuciak, J. A.; Chapin, D. S.; Harms, J. F.; Lebel, L. A.; McCarthy, S. A.; Chambers, L.; Shrikhande, A.; Wong, S.; Menniti, F. S.; Schmidt, C. J. *Neuropharmacology* **2006**, *51*, 386.
(29) Siuciak, J. A.; McCarthy, S. A.; Chapin, D. S.; Fujiwara, R. A.; James, L. C.; Williams, R. D.; Stock, J. L.; McNeish, J. D.; Strick, C. A.; Menniti, F. S.; Schmidt, C. J. *Neuropharmacology* **2006**, *51*, 374.
(30) Rodefer, J. S.; Murphy, E. R.; Baxter, M. G. *Eur. J. Neurosci.* **2005**, *21*, 1070.
(31) Soderling, S. H.; Bayuga, S. J.; Beavo, J. A. *Proc. Natl. Acad. Sci. U.S.A.* **1999**, *96*, 7071.
(32) Fujishige, K.; Kotera, J.; Michibata, H.; Yuasa, K.; Takebayashi, S.; Okumura, K.; Omori, K. *J. Biol. Chem.* **1999**, *274*, 18438.
(33) Loughney, K.; Snyder, P. B.; Uher, L.; Rosman, G. J.; Ferguson, K.; Florio, V. A. *Gene* **1999**, *234*, 109.

(34) Yathindra, N.; Sundaralingm, M. *Biochem. Biophys. Res. Commun.* **1974**, *56*, 119.
(35) Salter, E. A.; Wierzbicki, A.; Sperl, G.; Thompson, W. J. *Int. J. Quantum Chem.* **2004**, *96*, 402.
(36) Lawrenz, M. E.; Salter, E. A.; Wierzbicki, A.; Thompson, W. J. *Int. J. Quantum Chem.* **2005**, *105*, 410.
(37) Salter, E. A.; Wierzbicki, A. *J. Phys. Chem. B* **2007**, *111*, 4547.
(38) O'Brien, K. A.; Salter, E. A.; Wierzbick, A. *Int. J. Quantum Chem.* **2007**, *107*, 2197.
(39) Salter, E. A.; O'Brien, K. A.; Edmunds, R. W.; Wierzbicki, A. *Int. J. Quantum Chem.* **2008**, *108*, 1189.
(40) Zagrovic, B.; van Gunsteren, W. F. *J. Chem. Theory Comput.* **2007**, *3*, 301.
(41) Hamza, A.; Zhan, C. G. *J. Phys. Chem. B* **2009**, *113*, 2896.
(42) Torrie, G. M.; Valleau, J. P. *J. Comput. Phys.* **1977**, *23*, 187.
(43) Frenkel, D.; Smit, B. *Understand Molecular Simulations from Algorithms to Applications*, 2nd ed.; Academic Press: San Diego, 2002.
(44) Case, D. A.; Darden, T. A.; Cheatham, T. E., III; Simmerling, C. L.; Wang, J.; Duke, R.; Luo, R.; Merz, K. M.; Pearlman, D. A.; Crowley, M.; Walker, R. C.; Zhang, W.; Wang, B.; Hayik, S.; Roitberg, A.; Seabra, G.; Wong, K. F.; Paesani, F.; Wu, X.; Brozell, S.; Tsui, V.; Gohlke, H.; Yang, L.; Tan, C.; Mongan, J.; Hornak, V.; Cui, G.; Beroza, P.; Mathews, D. H.; Schafmeister, C.; Ross, W. S.; Kollman, P. A. University of California, San Francisco: San Francisco, CA, 2006.
(45) Wang, J. M.; Wolf, R. M.; Caldwell, J. W.; Kollman, P. A.; Case, D. A. *J. Comput. Chem.* **2004**, *25*, 1157.
(46) Wang, J. M.; Wang, W.; Kollman, P. A.; Case, D. A. *J. Mol. Graphics Modell.* **2006**, *25*, 247.
(47) Jorgensen, W. L.; Chandrasekhar, J.; Maudra, J. D. *J. Chem. Phys.* **1983**, *79*, 926.
(48) Ryckaert, J.-P.; Ciccotti, G.; Berendsen, H. J. C. *J. Comput. Phys.* **1977**, *23*, 327.
(49) Kumar, S.; Bouzida, D.; Swedsen, R. H.; Kollman, P. A.; Rosenberg, J. M. *J. Comput. Chem.* **1992**, *13*, 1011.
(50) Huai, Q.; Colicelli, J.; Ke, H. M. *Biochemistry* **2003**, *42*, 13220.
(51) Butt, E.; Beltman, J.; Becker, D. E.; Jensen, G. S.; Rybalkin, S. D.; Jastorff, B.; Beavo, J. A. *Mol. Pharmacol.* **1995**, *47*, 340.
(52) Iffland, A.; Kohls, D.; Low, S.; Luan, J.; Zhang, Y.; Kothe, M.; Cao, Q.; Kamath, A. V.; Ding, Y. H.; Ellenberger, T. *Biochemistry* **2005**, *44*, 8312.
(53) Chappie, T. A.; Humphrey, J. M.; Allen, M. P.; Estep, K. G.; Fox, C. B.; Lebel, L. A.; Liras, S.; Marr, E. S.; Menniti, F. S.; Pandit, J.; Schmidt, C. J.; Tu, M. H.; Williams, R. D.; Yang, F. V. *J. Med. Chem.* **2007**, *50*, 182.
(54) Verhoest, P. R.; Chapin, D. S.; Corman, M.; Fonseca, K.; Harms, J. F.; Hou, X. J.; Marr, E. S.; Menniti, F. S.; Nelson, F.; O'Connor, R.; Pandit, J.; Proulx-LaFrance, C.; Schmidt, A. W.; Schmidt, C. J.; Suiciak, J. A.; Liras, S. *J. Med. Chem.* **2009**, *52*, 5188.
(55) Andersen, O. A.; Schonfeld, D. L.; Toogood-Johnson, I.; Felicetti, B.; Albrecht, C.; Fryatt, T.; Whittaker, M.; Hallett, D.; Barker, J. *Acta Crystallogr.* **2009**, *D65*, 872.

JP911156G